BULLETIN OF THE POLISH ACADEMY OF SCIENCES
TECHNICAL SCIENCES, Vol. 66, No. 4, 2018
DOI: 10.24425/124265

Different fractional order models for an experimental smart beam system

K.A. MARKOWSKI[1*], I. BIRS[2], C.I. MURESAN[2], and O. PRODAN[3]

[1] Warsaw University of Technology, Department of Electrical Engineering, ISEP, 75 Koszykowa St., 00-662 Warsaw, Poland
[2] Technical University of Cluj-Napoca, Dept. of Automation, 28 Memorandumului St., 400114 Cluj-Napoca, Romania
[3] Technical University of Cluj-Napoca, Dept. of Civil Engineering, 15C Daicoviciu St., 400020 Cluj-Napoca, Romania

Abstract. The applicability of fractional calculus in system engineering outperforms classic identification techniques due to its ability to depict physical phenomena with increased accuracy. The present study explores the increased accuracy and flexibility of a fractional order model applied to an experimental smart beam depicting an airplane wing. The paper details the fractional order system identification of the beam and explores the possibility of realization of the model.

Key words: realization, fractional calculus, fractional order system identification, smart beam system, digraph method.

1. Introduction

The ability of a model to accurately describe the physical properties and the behavior of a process is crucial for developing efficient control strategies. When compared to the classical, integer order system identification, a fractional order model of the process better describes the dynamics of the overall process. Fractional calculus based identification has been studied intensely in the last years, especially for processes that exhibit viscoelastic properties [1]. Accurate models have been obtained for non-Newtonian fluids [2,3], lung pathology in pulmonary diseases [4], HIV infection models [5], smart beam [6] and many more.

Fractional order identification techniques have been previously explored through complex mathematics such as using the Riemann-Liouville fractional derivatives [7], least-square method and instrumental variable [8], continuous order-distributions [9] or optimization algorithms such as particle swarm optimization (PSO) [10].

In this paper, a fractional order transfer function is used to describe the model of a smart beam equipped with piezoelectric sensors and actuators. The beam is fixed at one end and it is left to freely vibrate at the other end. The aluminum beam has a viscoelastic characteristic that makes it fit for fractional order modeling. An experimental fractional order identification is presented based on the frequency domain magnitude of the oscillations.

The main purpose of this paper is to present a method, which will allow us to determine all possible realizations of the smart beam system using digraph theory. As a result, we have proposed the digraph-structure in the class $\mathcal{K}_1$. The digraphs classes in [11] have been defined and presented in detail. It should be noted, that for the first time in the papers [12] and [13] the use of digraph theory to analyze dynamical systems was proposed. Since then, more and more scientists try to use this theory in research, for example: electrical circuits [14, 15], kinetic of compartmental system [16], descriptor systems [17, 18].

This work has been organized as follows. Section 2 presents the identification process of the smart beam system. Then, in Sec. 3 different fractional order models are introduced. Elementary properties of the one- and two-dimensional digraph theory used to determine realization of the different fractional order models are presented in Sec. 4. In Sec. 5 the method used to determine the variable fractional order model and its realization has been presented in details. Finally, we propose some concluding remarks and outline problems open to further studies.

2. Fractional order identification

An integer order model of the smart beam has been determined experimentally by exciting the beam with a sinusoidal input of frequency 14.45 Hz and amplitude 1 V. The model obtained is given by

$$H(s) = \frac{1}{0.0128s^2 + 0.0156s + 104.94}. \tag{1}$$

The fit of the model (1) can be seen in Fig. 1. As can be seen, the model accurately describes the dynamics of the beam, but only at the frequency at which the identification was performed. A simple second order integer order model is unable to approximate the physical output at any given frequency; thus a more reliable model is needed.

The viscoelastic characteristic of the smart beam makes it suitable for a fractional order identification. The identification is performed assuming the following model

$$H_{FO}(s) = \frac{1}{a_1 s^2 + a_2 s^\alpha + a_3}, \tag{2}$$

*e-mail: Konrad.Markowski@ee.pw.edu.pl

Manuscript submitted 2017-11-22, revised 2018-01-27, initially accepted for publication 2018-01-29, published in August 2018.

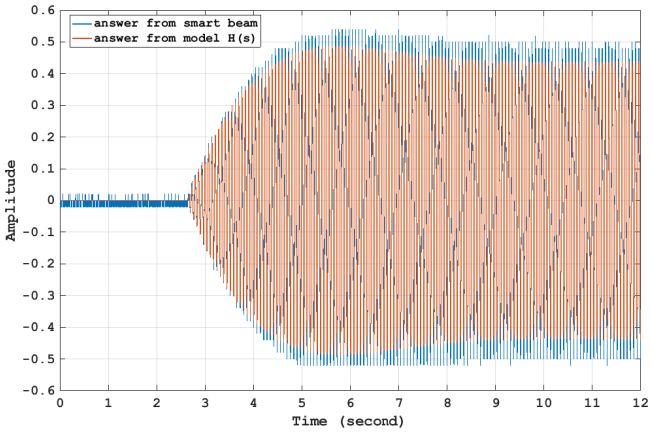

Fig. 1. Experimental identification of an integer order model overlaid on experimental data

where a_1, a_2 and a_3 are real coefficients and α is the non-integer power of the Laplace operator, s. The fractional model is identified through the four parameters. Mapping the Laplace to the frequency domain by replacing $s = j\omega$ in (2) and expanding the model further in its trigonometric form gives

$$H_{FO}(j\omega) = \frac{1}{-a_1\omega^2 + a_2\omega^\alpha \cos\frac{\alpha\pi}{2} + a_3 + ja_2\omega^\alpha \sin\frac{\alpha\pi}{2}}. \quad (3)$$

Replacing in (3) the real part with $\Re(\omega)$ and the imaginary one with $\Im(\omega)$

$$\begin{aligned} \Re(\omega) &= -a_1\omega^2 + a_2\omega^\alpha \cos\frac{\alpha\pi}{2} + a_3, \\ \Im(\omega) &= a_2\omega^\alpha \sin\frac{\alpha\pi}{2}, \end{aligned} \quad (4)$$

the magnitude and phase equations can be written as

$$\begin{aligned} |H_{FO}(j\omega)| &= \frac{1}{\sqrt{\Re(\omega)^2 + \Im(\omega)^2}}, \\ \angle H_{FO}(j\omega) &= \arctan\frac{\Im(\omega)}{\Re(\omega)}. \end{aligned} \quad (5)$$

The equations from (5) are estimated to experimentally determine the transfer function using the smart beam response of sinusoidal inputs of amplitude 1 V and different frequencies. The frequencies applied to the input are $f = [13, 13.97, 14.15, 14.34, 14.52, 14.71, 14.9, 15.08, 15.27, 15.46, 15.83, 16, 16.95, 18.07]$ Hz. For every test, the amplitude and phase are read experimentally and the system of equations from (5) becomes a system of two equations with two unknown parameters. Solving the system with classical methods may not lead to a solution and an optimization routine is recommended to obtain the final result. The *fmincon* function from MATLAB's Optimization Toolbox can be used to minimize the cost function, denoted by:

$$J = \min(|H_{FO}(j\omega_r)| - M_{\omega_r}(j\omega_r)) \Rightarrow \underbrace{\omega_r = 90.792^{\text{rad/s}}}_{f_r = 14.45 \text{ Hz}}, \quad (6)$$

where $M_{\omega_r}(j\omega_r)$ is the modulus of the smart beam at the resonant frequency $f_r = 14.45$ Hz as computed from experimental data.

Optimization algorithms start searching for the optimal solution from an initial point. The starting point is chosen based on analyzing the plausible solutions that can be obtained. Choosing different starting points may lead to different solutions.

The obtained optimal fractional order transfer function is

$$H_{FO}(s) = \frac{1}{0.0131s^2 + 0.027s^{0.89} + 107.72}. \quad (7)$$

The simulated results using the fractional model compared to the experimental data is shown in Fig. 2. The resonant frequency magnitude and the magnitudes enclosing it are accurately approximated using the obtained fractional model.

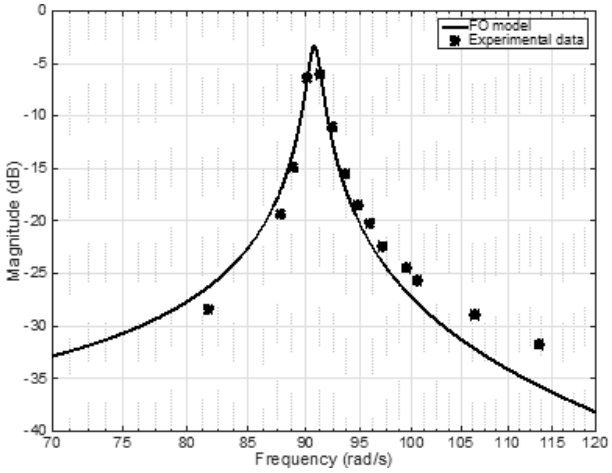

Fig. 2. Frequency response of the fractional order model and experimental data

A comparison between the fractional and integer order models is realized through performance indices.

$$P = \sum_{i=1}^{n} (y_{\exp}(i) - y_s(i))^2. \quad (8)$$

The obtained results in terms of the performance measurement is detailed in Table 1.

Table 1
Comparative performance results

f [Hz]	J as in (8)	
	FO model (1)	IO model (7)
13.00	1.73	2.13
13.97	6.70	10.77
14.15	13.87	27.14
14.34	19.35	40.53
14.52	5.18	14.74
14.57	3.76	5.96
14.71	17.99	21.03
14.90	9.19	10.27
15.27	4.66	4.96
16.00	1.92	1.97
[12,...,16]	6.57	10.3

Another experimental validation of the fractional and integer order models is realized for a sinusoidal input of variable

frequencies between 12 Hz and 16 Hz in Fig. 3. The fit obtained through the FO model better captures the dynamics of smart beam when compared to the integer order one. Near the resonant frequency, the fit obtained through the fractional model outperforms the integer order one by 65%.

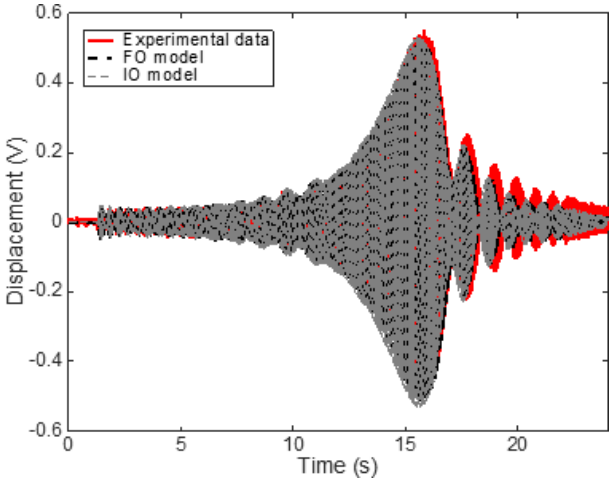

Fig. 3. Integer and fractional order validation of the obtained models on experimental data obtained through a swept sine between [12, 16] Hz

3. Different fractional order models

Let us consider a fractional matrix linear system [19] described by the equation:

$$\begin{bmatrix} {}_0^C\mathfrak{D}_t^{\alpha_1} x_1(t) \\ \vdots \\ {}_0^C\mathfrak{D}_t^{\alpha_n} x_n(t) \end{bmatrix} = \begin{bmatrix} \mathbf{A}_{1,1} \cdots \mathbf{A}_{1,n} \\ \vdots \quad \ddots \quad \vdots \\ \mathbf{A}_{n,1} \cdots \mathbf{A}_{n,n} \end{bmatrix} \begin{bmatrix} x_1(t) \\ \vdots \\ x_n(t) \end{bmatrix} + \begin{bmatrix} \mathbf{B}_1 \\ \vdots \\ \mathbf{B}_n \end{bmatrix} u(t),$$
$$y(t) = \begin{bmatrix} \mathbf{C}_1 \cdots \mathbf{C}_n \end{bmatrix} \begin{bmatrix} x_1(t) \\ \vdots \\ x_n(t) \end{bmatrix}, \tag{9}$$

where $x_k(t) \in \mathbb{R}^{\overline{n}_k}$ for $k = 1, 2, \ldots, n$ are the state vectors, $\mathbf{A}_{k,j} \in \mathbb{R}^{\overline{n}_k \times \overline{n}_j}$, $\mathbf{B}_k \in \mathbb{R}^{\overline{n}_k \times m}$, $\mathbf{C}_k \in \mathbb{R}^{p \times \overline{n}_k}$ for $k, j = 1, 2, \ldots, n$ and $u(t) \in \mathbb{R}^m$ is the input vector.

In this paper the following Caputo definition of the fractional derivative will be used:

$${}_a^C\mathfrak{D}_t^{\alpha} = \frac{d^{\alpha} f(t)}{dt^{\alpha}} = \frac{1}{\Gamma(n-\alpha)} \int_a^t \frac{f^{(n)}(\tau)}{(t-\tau)^{\alpha+1-n}} d\tau, \tag{10}$$

where $\alpha \in \mathbb{R}$ is the order of a fractional derivative,

$$f^{(n)}(\tau) = \frac{d^n f(\tau)}{d\tau^n} \qquad \text{and} \qquad \Gamma(x) = \int_0^{\infty} e^{-t} t^{x-1} dt$$

is the gamma function.

The Laplace transform of the derivative-integral (10) has the form

$$\mathcal{L}\left[{}_0^C\mathfrak{D}_t^{\alpha} f(t) \right] = s^{\alpha} F(s) - \sum_{k=1}^{n} s^{\alpha-k} f^{(k-1)}(0^+), \tag{11}$$

where $F(s) = \mathcal{L}[f(t)]$. Using the Laplace transforms

$$X_k(s) = \mathcal{L}[x_k(t)], \qquad k = 1, 2, \ldots, n;$$
$$U(s) = \mathcal{L}[u(t)] \tag{12}$$

and (11) we can write (9) in the following form

$$\begin{bmatrix} \mathbf{I}_{\overline{n}_1} s^{\alpha_1} - \mathbf{A}_{1,1} & -\mathbf{A}_{1,2} & \cdots & -\mathbf{A}_{1,n} \\ -\mathbf{A}_{2,1} & \mathbf{I}_{\overline{n}_2} s^{\alpha_2} - \mathbf{A}_{2,2} \cdots & & -\mathbf{A}_{2,n} \\ \vdots & \vdots & \ddots & \vdots \\ -\mathbf{A}_{n,1} & -\mathbf{A}_{n,2} & \cdots \mathbf{I}_{\overline{n}_n} s^{\alpha_n} - \mathbf{A}_{n,n} \end{bmatrix} \begin{bmatrix} X_1(s) \\ X_2(s) \\ \vdots \\ X_n(s) \end{bmatrix}$$
$$= \begin{bmatrix} \mathbf{B}_1 \\ \mathbf{B}_2 \\ \vdots \\ \mathbf{B}_n \end{bmatrix} U(s) + \begin{bmatrix} \sum_{j_1=1}^{\overline{n}_1} s^{\alpha_1 - j_1} x_{1,0}^{j_1-1} \\ \sum_{j_2=1}^{\overline{n}_2} s^{\alpha_2 - j_2} x_{2,0}^{j_2-1} \\ \vdots \\ \sum_{j_n=1}^{\overline{n}_n} s^{\alpha_n - j_n} x_{n,0}^{j_n-1} \end{bmatrix}. \tag{13}$$

Equation (13) can be rewritten as

$$\begin{bmatrix} X_1(s) \\ X_2(s) \\ \vdots \\ X_n(s) \end{bmatrix} = \begin{bmatrix} \mathbf{I}_{\overline{n}_1} s^{\alpha_1} - \mathbf{A}_{1,1} & -\mathbf{A}_{1,2} & \cdots & -\mathbf{A}_{1,n} \\ -\mathbf{A}_{2,1} & \mathbf{I}_{\overline{n}_2} s^{\alpha_2} - \mathbf{A}_{2,2} \cdots & & -\mathbf{A}_{2,n} \\ \vdots & \vdots & \ddots & \vdots \\ -\mathbf{A}_{n,1} & -\mathbf{A}_{n,2} & \cdots \mathbf{I}_{\overline{n}_n} s^{\alpha_n} - \mathbf{A}_{n,n} \end{bmatrix}^{-1}$$
$$\times \left\{ \begin{bmatrix} \mathbf{B}_1 \\ \mathbf{B}_2 \\ \vdots \\ \mathbf{B}_n \end{bmatrix} U(s) + \begin{bmatrix} \sum_{j_1=1}^{\overline{n}_1} s^{\alpha_1 - j_1} x_{1,0}^{j_1-1} \\ \sum_{j_2=1}^{\overline{n}_2} s^{\alpha_2 - j_2} x_{2,0}^{j_2-1} \\ \vdots \\ \sum_{j_n=1}^{\overline{n}_n} s^{\alpha_n - j_n} x_{n,0}^{j_n-1} \end{bmatrix} \right\}. \tag{14}$$

After using (14) and

$$Y(s) = \mathbf{C}X(s), \qquad U(s) = \mathcal{L}[u(t)] \tag{15}$$

we can determine the transfer matrix in the following form:

$$\mathbf{T}(s) = \begin{bmatrix} \mathbf{C}_1 \ldots \mathbf{C}_n \end{bmatrix}$$
$$\times \begin{bmatrix} \mathbf{I}_{\overline{n}_1} s^{\alpha_1} - \mathbf{A}_{11} \ldots & -\mathbf{A}_{1,n} \\ \vdots \quad \ddots & \vdots \\ -\mathbf{A}_{n,1} \quad \ldots \mathbf{I}_{\overline{n}_1} s^{\alpha_n} - \mathbf{A}_{n,n} \end{bmatrix}^{-1} \begin{bmatrix} \mathbf{B}_1 \\ \vdots \\ \mathbf{B}_n \end{bmatrix}. \tag{16}$$

4. Digraphs

A directed graph (called also digraph) $\mathcal{D}$ consists of a nonempty finite set $\mathbb{V}(\mathcal{D})$ of elements called vertices and a finite set $\mathbb{A}(\mathcal{D})$ of ordered pairs of distinct vertices called arcs. We call $\mathbb{V}(\mathcal{D})$ the vertex set and $\mathbb{A}(\mathcal{D})$ the arc set of $\mathcal{D}$. We will often write $\mathcal{D} = (\mathbb{V}, \mathbb{A})$ which means that $\mathbb{V} = \{v_i : i \in \mathbb{Z}_+\}$

and $\mathbb{A} = \{(v_i, v_j) : i \in \mathbb{Z}_+, j \in \mathbb{Z}_+\}$ are the vertex set and arc set of $\mathcal{D}$, respectively.

A two-dimensional digraph $\mathcal{D}^{(2)}$ is a directed graph with two types of arcs and input flows. For the first time, this type of digraph was presented in [12].

Definition 1. A two-dimensional digraph $\mathcal{D}^{(2)}$ is sextuple $(s, \mathbb{V}, \mathfrak{A}_1, \mathfrak{A}_2, \mathfrak{B}_1, \mathfrak{B}_2)$ where s is the source, $\mathbb{V} = \{v_1, v_2, \dots v_n\}$ is the set of vertices, $\mathfrak{A}_1$ and $\mathfrak{A}_2$ are subsets of $\mathbb{V} \times \mathbb{V}$ whose elements are called $\mathfrak{A}_1$-arcs and $\mathfrak{A}_2$-arcs respectively, meanwhile $\mathfrak{B}_1$ and $\mathfrak{B}_2$are subsets of $s \times \mathbb{V}$ whose elements are called $\mathfrak{B}_1$-arcs and $\mathfrak{B}_2$-arcs respectively.

There are two types of representations of the directed graph: list and incidence matrix. In detail, they are presented in books [20]. In this paper, an incidence matrix representation will be used. There exists an arc from vertex v_j to vertex v_i if and only if (i, j)-th entry of the matrix is non-zero.

Remark 1. It should be noted that $\mathfrak{A}_k$-arcs and $\mathfrak{B}_k$-arcs $(k = 1, 2)$, are drawn by the other colour or line style.

Example 1. For the system described by the matrices

$$\mathbf{A}_1 = \begin{array}{c} {}_{v_i}\backslash^{v_j} \\ v_1 \\ v_2 \\ v_3 \end{array} \begin{array}{c} \begin{array}{ccc} v_1 & v_2 & v_3 \end{array} \\ \begin{bmatrix} 1 & 0 & 0 \\ 0 & 0 & 1 \\ 1 & 0 & 0 \end{bmatrix} \end{array}, \tag{17}$$

$$\mathbf{A}_2 = \begin{array}{c} {}_{v_i}\backslash^{v_j} \\ v_1 \\ v_2 \\ v_3 \end{array} \begin{array}{c} \begin{array}{ccc} v_1 & v_2 & v_3 \end{array} \\ \begin{bmatrix} 0 & 0 & 1 \\ 1 & 0 & 0 \\ 0 & 1 & 0 \end{bmatrix} \end{array}$$

we can draw digraph $\mathcal{D}^{(2)}$, presented in Fig. 4, consisting of the set of vertices $\mathbb{V} = \{v_1, v_2, v_3\}$ and set of arcs $\mathbb{A} = \{(v_1, v_1)_{\mathfrak{A}_1}, (v_1, v_3)_{\mathfrak{A}_1}, (v_3, v_2)_{\mathfrak{A}_1}, (v_1, v_2)_{\mathfrak{A}_2}, (v_2, v_3)_{\mathfrak{A}_2}, (v_3, v_1)_{\mathfrak{A}_2}\}$.

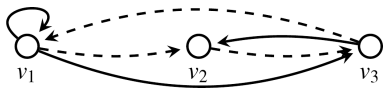

Fig. 4. Two-dimensional digraph $\mathcal{D}^{(2)}$ corresponding to matrices (17)

Some basic definitions from digraph theory which are used for further considerations will be presented below. A ***walk*** in a digraph $\mathcal{D}$ is a finite sequence of arcs in which every two vertices v_i and v_j are adjacent or identical. In Fig. 4 there is the following walk: $(v_1, v_2)_{\mathfrak{A}_2} \rightarrow (v_2, v_3)_{\mathfrak{A}_2} \rightarrow (v_3, v_2)_{\mathfrak{A}_1} \rightarrow (v_2, v_3)_{\mathfrak{A}_2}$. A walk in which all of the arcs are distinct is called a ***path***. In Fig. 4 there is the following path: $(v_1, v_1)_{\mathfrak{A}_1} \rightarrow (v_1, v_3)_{\mathfrak{A}_1}$. The path, that goes through all vertices, is called a ***finite path***. In Fig. 4 there is the following finite path: $(v_1, v_3)_{\mathfrak{A}_1} \rightarrow (v_3, v_2)_{\mathfrak{A}_1}$. If the initial and the terminal vertices of the path are the same, then the path is called a ***cycle***. In Fig. 4 there is the following cycle: $(v_1, v_1)_{\mathfrak{A}_1}$ or $(v_1, v_2)_{\mathfrak{A}_2} \rightarrow (v_2, v_3)_{\mathfrak{A}_2} \rightarrow (v_3, v_1)_{\mathfrak{A}_2}$. More information about digraph theory is provided in [20] and [21].

5. Realization problem

Let transfer function be described by the equation (7), which can be rewritten in its equivalent form:

$$H_{FO}(s) = \frac{76.3359}{s^2 + 2.0611 s^{0.89} + 8222.9}. \tag{18}$$

Taking into account that each power can be represented as a sum of powers, therefore we can decompose s^2 and $s^{0.89}$ as:

$$s^{0.89} \qquad \text{and} \qquad s^2 = s^{0.22} \cdot s^{0.89} \cdot s^{0.89}. \tag{19}$$

In this case we the have linear system consisting of two subsystems with different fractional orders equal to $\alpha_1 = 0.22$ and $\alpha_2 = 0.89$ in the following form:

$$\begin{bmatrix} {}_0^C\mathfrak{D}_t^{0.22} x_1(t) \\ {}_0^C\mathfrak{D}_t^{0.89} x_2(t) \end{bmatrix} = \begin{bmatrix} \mathbf{A}_{1,1} \mathbf{A}_{1,2} \\ \mathbf{A}_{2,1} \mathbf{A}_{2,2} \end{bmatrix} \begin{bmatrix} x_1(t) \\ x_2(t) \end{bmatrix} + \begin{bmatrix} \mathbf{B}_1 \\ \mathbf{B}_2 \end{bmatrix} u(t),$$
$$y(t) = \begin{bmatrix} \mathbf{C}_1 \mathbf{C}_2 \end{bmatrix} \begin{bmatrix} x_1(t) \\ x_2(t) \end{bmatrix}. \tag{20}$$

The transfer function of the system (20) is given by:

$$H_{FO}(s) = \begin{bmatrix} \mathbf{C}_1 \, \mathbf{C}_2 \end{bmatrix} \times \begin{bmatrix} \mathbf{I}_{n_1} s^{0.22} - \mathbf{A}_{1,1} & -\mathbf{A}_{1,2} \\ -\mathbf{A}_{2,1} & \mathbf{I}_{n_2} s^{0.89} - \mathbf{A}_{2,2} \end{bmatrix}^{-1} \begin{bmatrix} \mathbf{B}_1 \\ \mathbf{B}_2 \end{bmatrix}. \tag{21}$$

It should be noted that model (20) and its transfer function (21) is similar to Roesser model, which is well known in two-dimensional system theory [22]. Transfer function (21) can be considered as a pseudo-rational function of the variables $\lambda_1 = s^{0.22}$ and $\lambda_2 = s^{0.89}$ in the form:

$$H_{FO}(\lambda_1, \lambda_2) = \frac{n(\lambda_1, \lambda_2)}{d(\lambda_1, \lambda_2)}$$
$$= \begin{bmatrix} \mathbf{C}_1 \, \mathbf{C}_2 \end{bmatrix} \underbrace{\begin{bmatrix} \mathbf{I}_{n_1} \lambda_1 - \mathbf{A}_{1,1} & -\mathbf{A}_{1,2} \\ -\mathbf{A}_{2,1} & \mathbf{I}_{n_2} \lambda_2 - \mathbf{A}_{2,2} \end{bmatrix}^{-1}}_{\mathbf{F}(\lambda_1, \lambda_2)} \begin{bmatrix} \mathbf{B}_1 \\ \mathbf{B}_2 \end{bmatrix}$$
$$= \frac{\begin{bmatrix} \mathbf{C}_1 \, \mathbf{C}_2 \end{bmatrix} \operatorname{Adj} \mathbf{F}(\lambda_1, \lambda_2) \begin{bmatrix} \mathbf{B}_1 \\ \mathbf{B}_2 \end{bmatrix}}{\det \mathbf{F}(\lambda_1, \lambda_2)} \tag{22}$$
$$= \frac{76.3359}{\lambda_1^2 \lambda_1 + 2.0611 \lambda_1 + 8222.9}$$

where the characteristic polynomial has the following form:

$$d(\lambda_1, \lambda_2) = \det \left[\mathbf{I} \lambda_1 \lambda_2 - \mathbf{A}_{2,2} \lambda_1 - \mathbf{A}_{1,1} \lambda_2 - (\mathbf{A}_{1,2} \mathbf{A}_{2,1} - \mathbf{A}_{1,1} \mathbf{A}_{2,2}) \right]. \tag{23}$$

After multiplying transfer function (22) by $\lambda_1^{-2} \lambda_2^{-1}$ we obtain the characteristic polynomial in the equivalent form

$$d(\lambda_1, \lambda_2) = 1 + 2.0611 \lambda_1^{-1} \lambda_2^{-1} + 8222.9 \lambda_1^{-2} \lambda_2^{-1}. \tag{24}$$

In the next step to determine the state matrices $\mathbf{A}_{1,1}$, $\mathbf{A}_{1,2}$, $\mathbf{A}_{2,1}$ and $\mathbf{A}_{2,2}$ we can transform Roesser model to the second

Fornasini-Marechesini model (IIF-M), which has the following structure:

$$\begin{aligned}\frac{\partial^2 x(t_1,t_2)}{\partial t_1 \partial t_2} &= \mathbf{A}_1 \frac{\partial x(t_1,t_2)}{\partial t_1} + \mathbf{A}_2 \frac{\partial x(t_1,t_2)}{\partial t_2} \\ &+ \mathbf{B}_1 \frac{\partial u(t_1,t_2)}{\partial t_1} + \mathbf{B}_2 \frac{\partial u(t_1,t_2)}{\partial t_2}, \\ y(t_1,t_2) &= \mathbf{C} x(t_1,t_2).\end{aligned} \tag{25}$$

The transfer function, consisting of two variables λ_1 and λ_2, corresponding to (25) has the form:

$$\begin{aligned}T(\lambda_1,\lambda_2) &= \frac{n(\lambda_1,\lambda_2)}{d(\lambda_1,\lambda_2)} \\ &= \mathbf{C}\left[\mathbf{I}\lambda_1\lambda_2 - \mathbf{A}_1\lambda_1 - \mathbf{A}_2\lambda_2\right]^{-1}(\mathbf{B}_1\lambda_1 + \mathbf{B}_2\lambda_2),\end{aligned} \tag{26}$$

where

$$\widetilde{d}(\lambda_1,\lambda_2) = \det\left(\mathbf{I}\lambda_1\lambda_2 - \mathbf{A}_1\lambda_1 - \mathbf{A}_2\lambda_2\right) \tag{27}$$

is the characteristic polynomial. Comparing (23) with (27) we obtain the following relations:

$$\begin{aligned}\mathbf{A}_{2,2} &= \mathbf{A}_1, \qquad \mathbf{A}_{1,1} = \mathbf{A}_2, \\ \mathbf{A}_{1,2}\mathbf{A}_{2,1} &- \mathbf{A}_{1,1}\mathbf{A}_{2,2} = 0.\end{aligned} \tag{28}$$

It should be noted that relation (28) results from structure of the characteristic polynomial (27) of the second Fornasini-Marchesini model and it is easy to determine. If conditions (28) are satisfied then characteristic polynomials (23) and (27) are equivalents and $d(\lambda_1,\lambda_2) \equiv \widetilde{d}(\lambda_1,\lambda_2)$.

After multiplying denominator of the transfer function (26) by $\lambda_1^{-1}\lambda_2^{-1}$ we can write characteristic polynomial (27) in the following form

$$\widetilde{d}(\lambda_1,\lambda_2) = \det\left(\mathbf{I} - \mathbf{A}_1\lambda_2^{-1} - \mathbf{A}_2\lambda_1^{-1}\right). \tag{29}$$

Comparing (24) with (29) we obtain characteristic polynomial:

$$\widetilde{d}(\lambda_1,\lambda_2) = 1 + 2.0611\lambda_1^{-1}\lambda_2^{-1} + 8222.9\lambda_1^{-2}\lambda_2^{-1}. \tag{30}$$

The equation (30) can be written as a sum of binomials in the following form:

$$\widetilde{d}(\lambda_1,\lambda_2) = \underbrace{(1+2.0611\lambda_1^{-1}\lambda_2^{-1})}_{B_{11}=1-d_{11}\lambda_1^{-1}\lambda_2^{-1}} \cup \underbrace{(1+8222.9\lambda_1^{-2}\lambda_2^{-1})}_{B_{21}=1-d_{21}\lambda_1^{-2}\lambda_2^{-1}}. \tag{31}$$

For each binomial B_{11} and B_{21} from (31), we must create all possible two-dimensional digraphs representations using Proposition 1. We will assume further that: arcs corresponding to matrix $\mathbf{A}_1$ are drawn by the solid line and we assign the weight $w(v_i,v_j)_{\mathfrak{A}_1}\lambda_2^{-1}$, $i,j \in \mathbb{Z}_+$; arcs corresponding to matrix $\mathbf{A}_2$ are drawn by the dashed line and we assign the weight $w(v_i,v_j)_{\mathfrak{A}_2}\lambda_1^{-1}$, $i,j \in \mathbb{Z}_+$. It should be noted that in arc weight $\mathfrak{A}_1$ and $\mathfrak{A}_2$ is label corresponding to state matrix $\mathbf{A}_1$ and $\mathbf{A}_2$ respectively.

Proposition 1. The digraph corresponding to binomial $B_k = 1 - a_{k,l}\lambda_1^{-k}\lambda_2^{-l}$ where $k = 0,1,\ldots,n$; $l = 0,1,\ldots,n$; $0 < k+l \leq n$ consisting of one cycle contains $(k+l)$-arcs where l corresponding to $\mathfrak{A}_1$-arcs and k corresponding to $\mathfrak{A}_2$-arcs.

Proof. Suppose that the two-dimensional digraph $\mathcal{D}^2$ consists of the following vertices: $v_1, v_2, \ldots, v_{n-1}, v_n$. For each of the arcs in the digraph we assigned weights $w(v_i,v_j)_{\mathfrak{A}_2}\lambda_1^{-1}$ or $w(v_i,v_j)_{\mathfrak{A}_1}\lambda_2^{-1}$ for $i,j \in \mathbb{Z}_+ = \{1,2,\ldots,n\}$. Let us consider the boundary points in the set:

- *Lower boundary:* If $k = 0$ and $l = 1$, then the power of the binomial is equal to $a_{0,1}\lambda_2^{-1}$. The cycle consist from one arc and can be written as $w(v_i,v_j)_{\mathfrak{A}_1}\lambda_2^{-1}$, for $i = j$. The dual boundary point is for $k = 1$ and $l = 0$.
- *Upper boundary:* If $k = 0$ and $l = n$, then the power of the binomial is equal to $a_{0,n}\lambda_2^{-n}$. The cycle can be written as $w(v_1,v_2)_{\mathfrak{A}_1}\lambda_2^{-1},\ldots,w(v_i,v_j)_{\mathfrak{A}_1}\lambda_2^{-1},w(v_j,v_1)_{\mathfrak{A}_1}\lambda^{-1}$. In this case the maximum weight in a digraph is equal to $[w(v_1,v_2)_{\mathfrak{A}_1}\cdot\ldots\cdot w(v_{i-1},v_j)_{\mathfrak{A}_1}\cdot w(v_j,v_1)_{\mathfrak{A}_1}]\lambda_2^{-n} = a_{0,n}\lambda_2^{-n}$. The dual boundary point is for $k = n$ and $l = 0$
- *Upper boundary:* If $k = 1$ and $l = n-1$, then the power of the binomial is equal to $a_{1,n-1}\lambda_1^{-1}\lambda_2^{-n+1}$. The cycle can be written for example as $w(v_1,v_2)_{\mathfrak{A}_2}\lambda_1^{-1},\ldots,w(v_i,v_j)_{\mathfrak{A}_1}\lambda_2^{-1},w(v_j,v_1)_{\mathfrak{A}_1}\lambda^{-1}$. In this case the maximum weight in a digraph is equal to $[w(v_1,v_2)_{\mathfrak{A}_2}\cdot\ldots\cdot w(v_{i-1},v_j)_{\mathfrak{A}_1}\cdot w(v_j,v_1)_{\mathfrak{A}_1}]\lambda_1^{-1}\lambda_2^{-n+1} = a_{1,n-1}\lambda_1^{-1}\lambda_2^{-n+1}$. In this case the sum of the power is equal to n. It should be noted that weight $w(v_i,v_j)_{\mathfrak{A}_2}\lambda_1^{-1}$ can be at any position in the cycle. The dual boundary point is for $k = n-1$ and $l = 1$

□

From Proposition 1 we can determine binomial: B_{11} realization presented in Fig. 5a and B_{21} realization presented in Fig. 5b.

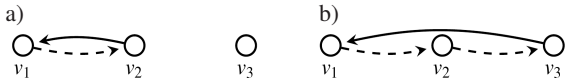

Fig. 5. Digraph corresponding to binomial: a) B_{11}; b) B_{21}

Remark 2. It should be noted that all possible realizations of the binomials B_{11} and B_{21} can be obtained the digraphs presented in Fig. 5a and 5b respectively by:

- **Renumbering vertices in the digraph**. This operation is similar to a circle rotation and is synonymous with swapping columns/rows of a matrix that is used in the matrix theory. The results of this operation for the digraph from Fig. 5a are presented in Fig. 6a–b and for the digraph from Fig. 5b are presented in Fig. 6c–d.

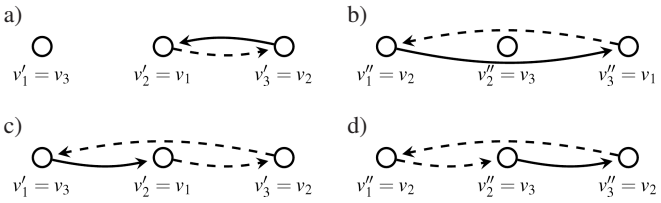

Fig. 6. Renumbering vertices in digraph

- **Change of the direction of the arcs in the digraph**. This operation is similar to a transposition matrix used in the matrix theory. The results of this operation for digraphs from Figs. 5a, 6a–b are presented in Fig. 7a–c and for digraphs from Figs. 5b, 6c–d are presented in Fig. 7d–f.

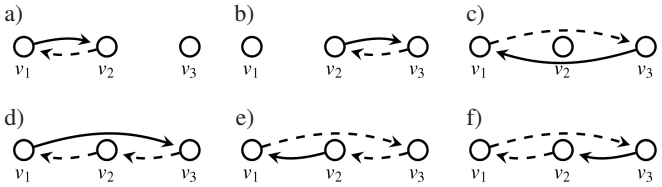

Fig. 7. Change of the direction of the arcs in the digraph

The following definition is introduced for the operation of the composition relative to vertices on digraphs and will be used in further considerations.

Definition 2. Let $\mathcal{G}_1, \mathcal{G}_2, \cdots, \mathcal{G}_n$ be a digraph with vertex sets $\mathbb{V}(\mathcal{G}_n) = \{v_{i(n)} : i \in \mathbb{Z}_+\}$. The composition relative to vertices $\mathcal{D}[\mathcal{G}_1, \mathcal{G}_2, \cdots, \mathcal{G}_n]$ is the two-dimensional digraph $\mathcal{L}^{(2)} = (\mathbb{V}, \mathbb{A}')$ with vertex set $\mathbb{V}(\mathcal{G}_1) \cup \mathbb{V}(\mathcal{G}_2) \cup \cdots \cup \mathbb{V}(\mathcal{G}_n) = \{v_j : j = 1, \cdots, \max\{i(n)\}, i \in \mathbb{Z}_+\}$ and arc set $\mathbb{A}'(\mathcal{L}) = \mathbb{A}(\mathcal{G}_1) \cup \mathbb{A}(\mathcal{G}_2) \cup \cdots \cup \mathbb{A}(\mathcal{G}_n)$, where $'$ denotes the operation of deleting multiple arcs with this same label.

Example 2. Let be given two digraphs $\mathcal{G}_1$ (see Fig. 8a) corresponding to binomial $B_{03} = 1 \mp \lambda_2^{-3}$ and $\mathcal{G}_2$ (see Fig. 8b) corresponding to binomial $B_{11} = 1 \mp \lambda_1^{-1}\lambda_2^{-1}$ with the set of vertex $\mathbb{V}(\mathcal{G}_1) = \{v_{1(1)}, v_{2(1)}, v_{3(1)}\}$ and $\mathbb{V}(\mathcal{G}_2) = \{v_{1(2)}, v_{2(2)}\}$. The composition relative to vertices creates a new digraph $\mathcal{L}$, and it consists of a vertex set $\mathbb{V}(\mathcal{L}) = \mathbb{V}(\mathcal{G}_1) \cup \mathbb{V}(\mathcal{G}_2) = \{v_1, v_2, v_3\}$ and arc set $\mathbb{A}'(\mathcal{L})$. In Fig. 9, we have presented all possible realizations of digraphs after using a composition relative to vertices.

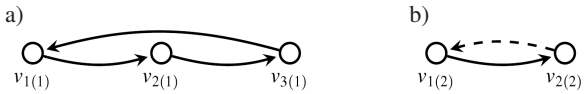

Fig. 8. Two-dimensional digraph: a) $\mathcal{G}_1$; b) $\mathcal{G}_2$

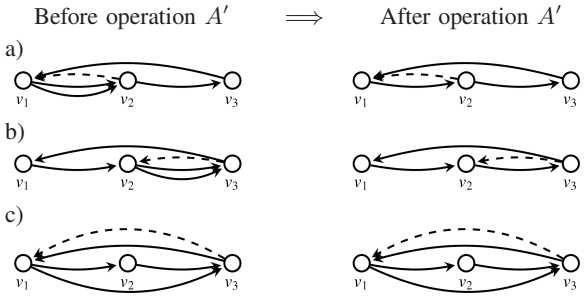

Fig. 9. Composition relative to vertices

Then using Proposition 1, Definition 2 and Theorem 2 presented in [23] and [24], we can create all possible digraphs representations (in class $\mathcal{K}_1$) of the characteristic polynomial (30). For considered polynomial we have 36 possible realizations. Each digraph corresponding to a characteristic polynomial must satisfy two conditions. The first condition (C1) relates to the existence in the common part of the digraph (vertex in black), the second condition (C2) relates to non-existence of additional cycles in the digraph. Finally, we have 18 possible digraphs structures. In Fig. 10, three realizations are presented; the next six realizations are obtained by renumbering vertices in digraphs; other nine realizations are obtained by changing all arcs directions in digraphs.

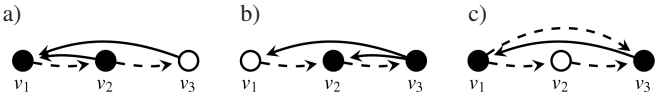

Fig. 10. Three digraph structures corresponding to polynomial (30)

From all the potential proper realizations, we choose the realization presented in Fig. 11, to present in detail.

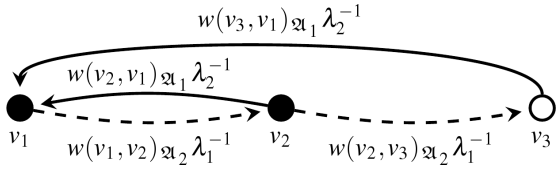

Fig. 11. Full digraph-structure corresponding to polynomial (30)

For considered digraph-structure we can write the following set of the equations:

$$\begin{cases} \lambda_1^{-1}\lambda_2^{-1} \| w(v_1, v_2)_{\mathfrak{A}_2} \cdot w(v_2, v_1)_{\mathfrak{A}_1} = -2.0611 \\ \lambda_1^{-2}\lambda_2^{-1} \| w(v_1, v_2)_{\mathfrak{A}_2} \cdot w(v_2, v_3)_{\mathfrak{A}_2} \cdot \\ \qquad\qquad \| \cdot w(v_3, v_1)_{\mathfrak{A}_1} = -8222.9 \ . \end{cases} \tag{32}$$

After solving (32), we obtain the following weights of digraph arcs:

$$\begin{aligned} w(v_2, v_1)_{\mathfrak{A}_1} &= \frac{-2.0611}{w(v_1, v_2)_{\mathfrak{A}_2}}, \\ w(v_3, v_1)_{\mathfrak{A}_1} &= \frac{-8222.9}{w(v_1, v_2)_{\mathfrak{A}_2}\, w(v_2, v_3)_{\mathfrak{A}_2}}. \end{aligned} \tag{33}$$

Remark 3. It should be noted that the set of equations (32) has many solutions (33) which depend on weights: $w(v_1, v_2)_{\mathfrak{A}_2} \in \mathbb{R}$ and $w(v_2, v_3)_{\mathfrak{A}_2} \in \mathbb{R}$. The proposed solution

$$\begin{aligned} w(v_1, v_2)_{\mathfrak{A}_2} &= 1, \qquad w(v_2, v_1)_{\mathfrak{A}_1} = -2.0611, \\ w(v_2, v_3)_{\mathfrak{A}_2} &= 1, \qquad w(v_3, v_1)_{\mathfrak{A}_1} = -8222.9 \end{aligned} \tag{34}$$

is only one of the many possible. In addition, the solution does not depend on the structure and properties of the digraph presented in Fig. 11. Now we can write state matrices $\mathbf{A}_1$ and $\mathbf{A}_2$ in the following form:

$$\begin{aligned} \mathbf{A}_1 &= \begin{bmatrix} 0 & w(v_2, v_1)_{\mathfrak{A}_1} & w(v_3, v_1)_{\mathfrak{A}_1} \\ 0 & 0 & 0 \\ 0 & 0 & 0 \end{bmatrix} = \begin{bmatrix} 0 & -2.0611 & -8222.9 \\ 0 & 0 & 0 \\ 0 & 0 & 0 \end{bmatrix}, \\ \mathbf{A}_2 &= \begin{bmatrix} 0 & 0 & 0 \\ w(v_1, v_2)_{\mathfrak{A}_2} & 0 & 0 \\ 0 & w(v_2, v_3)_{\mathfrak{A}_2} & 0 \end{bmatrix} = \begin{bmatrix} 0 & 0 & 0 \\ 1 & 0 & 0 \\ 0 & 1 & 0 \end{bmatrix}. \end{aligned} \tag{35}$$

Then, by the using condition (28), we can write state matrices corresponding to the transfer function (22) in the following form:

$$\mathbf{A} = \left[\begin{array}{c|c} \underbrace{\mathbf{A}_{1,1}}_{\mathbf{A}_2\in\mathbb{R}^{3\times3}} & \underbrace{\mathbf{A}_{1,2}}_{\mathbf{A}_2\mathbf{A}_1\in\mathbb{R}^{3\times3}} \\ \hline \underbrace{\mathbf{A}_{2,1}}_{\mathbf{I}_3\in\mathbb{R}^{3\times3}} & \underbrace{\mathbf{A}_{2,2}}_{\mathbf{A}_1\in\mathbb{R}^{3\times3}} \end{array}\right]$$

$$= \left[\begin{array}{ccc|ccc} 0 & 0 & 0 & 0 & 0 & 0 \\ 1 & 0 & 0 & 0 & -2.0611 & -8222.9 \\ 0 & 1 & 0 & 0 & 0 & 0 \\ \hline 1 & 0 & 0 & 0 & -2.0611 & -8222.9 \\ 0 & 1 & 0 & 0 & 0 & 0 \\ 0 & 0 & 1 & 0 & 0 & 0 \end{array}\right]. \tag{36}$$

Remark 4. To determine state matrix $\mathbf{A}$ in the form (36):

- in the first stage we convert linear system consisting of two subsystems with different fractional orders (20) to two-dimensional linear second Fornasini-Marchesini model (25) and determine matrices $\mathbf{A}_1$ and $\mathbf{A}_2$
- in the second stage using condition (28), we convert two-dimensional linear second Fornasini-Marchesini model (25) to linear system consisting of two subsystems with different fractional orders (20).

Because we used twice conversion between models then to determine input matrix $\mathbf{B}$ and output matrix $\mathbf{C}$ we will use the digraph corresponding to the matrix (36), presented in Fig. 12. In the next step, we need to extend the obtained digraph by adding source vertex s and output vertex y. Then we connect source with output in such a way to obtain a path with weight equal to polynomial

$$n(\lambda_1,\lambda_2) = 76.3359\lambda_1^{-2}\lambda_2^{-1} \tag{37}$$

which we obtain by multiplying transfer function (22) by $\lambda_1^{-2}\lambda_2^{-1}$. We have four possible cases in which we connect source vertex s with vertex: v_1; v_2; v_5; v_6; and we connect vertices $v_1,\ldots,v_6$ with the output vertex y.

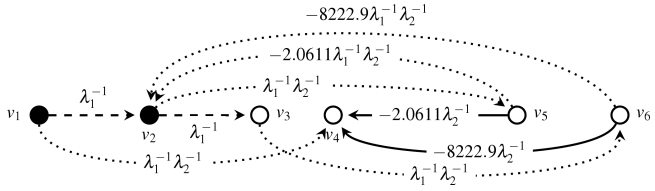

Fig. 12. Digraph corresponding to state matrix (36)

Below we will consider in detail Case 1 in which we connect source vertex s with vertex v_1 and vertices $v_1,\ldots,v_6$ with the output vertex y. Then, we determine all paths from the source s to output vertex y. This kind of connection was presented in Fig. 13.

After using the composition relative to vertices (Definition 2) to digraphs presented in Figs. 13a–h, we obtain a digraph, presented in Fig. 14, corresponding to polynomial (37). Then, using the created digraph, we can write the set of equations (38) and after solving them, we receive the following weights of digraph:

$$w(v_1,y)=0,\quad w(v_2,y)=0,\quad w(v_3,y)=0,$$
$$w(v_4,y)=0,\quad w(v_5,y)=\frac{76.3359}{w(s,v_1)},\quad w(v_6,y)=0,$$

for $w(s,v_1)\in\mathbb{R}$. Now we can write matrices in the following form:

$$\mathbf{B} = \left[\begin{array}{c} w(s,v_1) \\ 0 \\ 0 \\ 0 \\ 0 \\ 0 \end{array}\right], \tag{39}$$

$$\mathbf{C} = \left[\begin{array}{cccccc} 0 & 0 & 0 & 0 & \dfrac{76.3359}{w(s,v_1)} & 0 \end{array}\right].$$

$$\left\{\begin{array}{lll} & w(s,v_1)w(v_1,y) & = 0 \\ \lambda_1^{-1} & w(s,v_1)w(v_1,v_2)w(v_2,y) & \Rightarrow w(s,v_1)w(v_2,y) = 0 \\ \lambda_1^{-2} & w(s,v_1)w(v_1,v_2)w(v_2,v_3)w(v_3,y) & \Rightarrow w(s,v_1)w(v_3,y) = 0 \\ \lambda_1^{-1}\lambda_2^{-1} & w(s,v_1)w(v_1,v_4)w(v_4,y) & \Rightarrow w(s,v_1)w(v_4,y) = 0 \\ \lambda_1^{-2}\lambda_2^{-1} & w(s,v_1)w(v_1,v_2)w(v_2,v_5)w(v_5,y) & \Rightarrow w(s,v_1)w(v_5,y) = 76.3359 \\ \lambda_1^{-2}\lambda_2^{-2} & -2.0611\cdot w(s,v_1)w(v_1,v_2)w(v_2,v_5)w(v_5,v_4)w(v_4,y) & \Rightarrow -2.0611\cdot w(s,v_1)w(v_4,y) = 0 \\ \lambda_1^{-3}\lambda_2^{-1} & w(s,v_1)w(v_1,v_2)w(v_2,v_3)w(v_3,v_6)w(v_6,y) & \Rightarrow w(s,v_1)w(v_6,y) = 0 \\ \lambda_1^{-3}\lambda_2^{-2} & -8222.9\cdot w(s,v_1)w(v_1,v_2)w(v_2,v_3)w(v_3,v_6)w(v_6,v_4)w(v_4,y) & \Rightarrow -8222.9\cdot w(s,v_1)w(v_4,y) = 0 \end{array}\right. \tag{38}$$

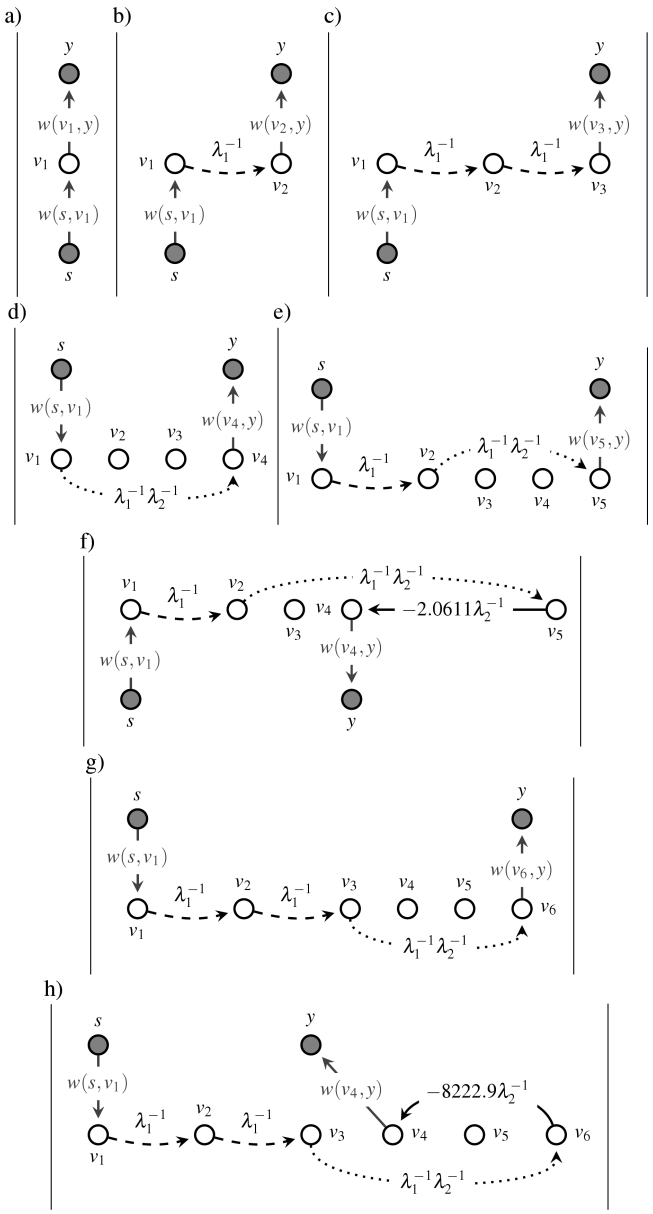

Fig. 13. All possible paths from source vertex s to output vertex y

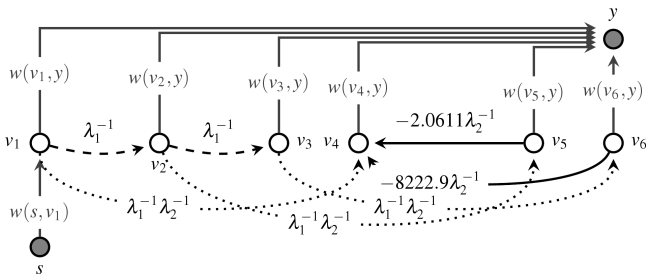

Fig. 14. Digraph corresponding to polynomial (37)

The desired realization $(\mathbf{A}, \mathbf{B}, \mathbf{C})$ of the smart beam system described by the transfer function (18) is given by the matrices (36) and (39) for $w(s, v_1) \in \mathbb{R}$.

Remark 5. It should be noted that the other cases we obtained by extending digraph-structure presented in Fig. 12 by connect $v_1, \ldots, v_6$ with output vertex y and source vertex s with: v_2 (Case 2); v_5 (Case 3); v_6 (Case 4). Method of determining the matrix $\mathbf{B}$, and $\mathbf{C}$ is the same as in Case 1.

6. Concluding remarks

A method which allows us to determine all possible realizations using two-dimensional digraph theory to the smart beam system has been described in this paper. It is shown in detail that based on the experimental identification of a smart beam system, it is possible to determine all possible realizations in an easy and straightforward way. Accordingly, a physical system can be described in state-space form. The considerations were presented for system identification in the form of fractional order (FO) model, under the assumption of a linear system consisting of two subsystems with different fractional orders. It should be noted that it is also possible to consider a general system consisting of n-subsystems with different fractional orders. In this case we can transform the model to a n-dimensional system. When the number of subsystems grows, the analysis of such a system becomes more complex.

Future work includes the extension of the method presented in this paper to obtain minimal realizations based on digraph theory for the switch fractional order model of the smart beam system.

Acknowledgements. This work was partially supported by a grant of the Romanian National Authority for Scientific Research and Innovation, CNCS UEFISCDI, project number PN-II- RU-TE-2014-4-0598, TE 86/2015; and partially supported by Statutory Research founds of Faculty of Electrical Engineering, Warsaw University of Technology.

REFERENCES

[1] F. Mainardi, *Fractional Calculus and Waves in Linear Viscoelasticity: An Introduction to Mathematical Models*, Imperial College Press, 2010, DOI: 10.1007/978-1-4419-6397-0.

[2] C.M. Ionescu, "A memory-based model for blood viscosity", *Communications in Nonlinear Science and Numerical Simulation* 45, 29–34 (2017), DOI: 10.1016/j.cnsns.2016.09.017.

[3] D. Tong, R. Wang, and H. Yang, "Exact solutions for the flow of non-Newtonian fluid with fractional derivative in an annular pipe", *Science in China Series G: Physics, Mechanics and Astronomy* 48(4), 485–495 (2005), DOI: 10.1360/04yw0105.

[4] C.M. Ionescu and R.D. Keyser, "Relations between fractional-order model parameters and lung pathology in chronic obstructive pulmonary disease", *IEEE Transactions on Biomedical Engineering* 56(4), 978–987 (2009).

[5] C.M. Pinto and A.R. Carvalho, "Fractional complex-order model for HIV infection with drug resistance during therapy", *Journal of Vibration and Control* 22(9), 2222–2239 (2016), DOI: 10.1177/1077546315574964.

[6] C. I. Muresan, S. Folea, I. Birs, and C. Ionescu, "Fractional order modeling and control of a smart beam," in *2017 IEEE Conference on Control Technology and Applications* pp. 1517–1523, 2017, DOI: 10.1109/CCTA.2017.8062672.

[7] D.-Y. Liu, L.-K. Taous-Meriem, O. Gibaru, and W. Perruquetti, "Identification of fractional order systems using modulating functions method", in *American Control Conference (ACC)*, pp. 1679–1684, 2013.

[8] A. Khadhraoui, K. Jelassi, J.-C. Trigeassou, and P. Melchior, "Identification of fractional model by least-squares method and instrumental variable", *Journal of Computational and Nonlinear Dynamics* 10(5), 2015, DOI: 10.1115/1.4029904.

[9] T.T. Hartley and C.F. Lorenzo, "Fractional-order system identification based on continuous order-distributions", *Signal Processing* 83(11), 2287–2300 (2003).

[10] D. Maiti, M. Chakraborty, and A. Konar, "A novel approach for complete identification of dynamic fractional order systems using stochastic optimization algorithms and fractional calculus", in *2008 International Conference on Electrical and Computer Engineering*, pp. 867–872, 2008.

[11] K. Hryniów and K.A. Markowski, "Classes of digraph structures corresponding to characteristic polynomials", in *Challenges in Automation, Robotics and Measurement Techniques*, Springer International Publishing, pp. 329–339, 2016, DOI: 10.1007/978-3-319-29357-8_30.

[12] E. Fornasini and M.E. Valcher, "Directed graphs, 2D state models, and characteristic polynomials of irreducible matrix pairs", *Linear Algebra and its Applications* 263, 275–310 (1997).

[13] E. Fornasini and M.E. Valcher, "Controllability and reachability of 2D positive systems: a graph theoretic approach", *IEEE Transaction on Circuits and Systems I* 52, 576–585 (2005).

[14] K.A. Markowski, "Digraphs structures corresponding to realisation of multi-order fractional electrical circuits", in *2016 IEEE International Conference on Automation, Quality and Testing, Robotics (AQTR)*, pp. 1–6, 2016, DOI: 10.1109/AQTR.2016.7501368.

[15] K.A. Markowski, *Relations Between Digraphs Structure and Analogue Realisations with an Example of Electrical Circuit*, Springer International Publishing, pp. 215–226, 2017, DOI: 10.1007/978-3-319-54042-9_20.

[16] K.A. Markowski, "Fractional kinetics of compartmental systems. First approach with use digraph-based method", *Proc. SPIE* 10445, 10445–10445–9 (2017), DOI: 10.1117/12.2281028.

[17] K.A. Markowski, "Realisation of linear continuous-time fractional singular systems using digraph-based method. First approach", *Journal of Physics: Conference Series* 783(1), 012052 (2017), DOI: 10.1088/1742-6596/783/1/012052.

[18] K.A. Markowski, "Minimal positive realizations of linear continuous-time fractional descriptor systems. two cases of input-output digraph-structure", *International Journal of Applied Mathematics and Computer Science* 28(1), 2018, (in press).

[19] T. Kaczorek and L. Sajewski, *The Realization Problem for Positive and Fractional Systems*, Springer Publishing, 2014.

[20] W.D. Wallis, *A Beginner's Guide to Graph Theory*, Biokhäuser, 2007.

[21] J. Bang-Jensen and G. Gutin, *Digraphs: Theory, Algorithms and Applications*, London: Springer-Verlag, 2009.

[22] R.B. Roesser, "A discrete state-space model for linear image processing", *IEEE Trans. Austom. Contr.* no. AC-20, pp. 1–10 (1975).

[23] K. Hryniów and K.A. Markowski, "Optimisation of digraphs creation for parallel algorithm for finding a complete set of solutions of characteristic polynomial", in *20th International Conference on Methods and Models in Automation and Robotics*, pp. 1139–1144, 2015, DOI: 10.1109/MMAR.2015.7284039.

[24] K.A. Markowski, "Determination of minimal realisation of one-dimensional continuous-time fractional linear system", *International Journal of Dynamics and Control* 5(1), 40–50 (2017), DOI: 10.1007/s40435-016-0232-3.